nanomaterials

MDPI

Review

Recent Advances in Synthesis, Medical Applications and Challenges for Gold-Coated Iron Oxide: Comprehensive Study

Mohammed Ali Dheyab [1,2,*], Azlan Abdul Aziz [1,2,*], Mahmood S. Jameel [1,2] and Pegah Moradi Khaniabadi [3]

[1] Nano-Biotechnology Research and Innovation (NanoBRI), Institute for Research in Molecular Medicine (INFORMM), Universiti Sains Malaysia, Pulau Pinang 11800, Malaysia; mahmood@student.usm.my
[2] Nano-Optoelectronics Research and Technology Lab (NORLab), School of Physics, Universiti Sains Malaysia, Pulau Pinang 11800, Malaysia
[3] Department of Radiology and Molecular Imaging, College of Medicine and Health Science, Sultan Qaboos University, P.O. Box 35, Al Khod, Muscat 123, Oman; p.khaniabadi@squ.edu.om
* Correspondence: mdali@usm.my (M.A.D.); lan@usm.my (A.A.A.)

Abstract: Combining iron oxide nanoparticles (Fe_3O_4 NPs) and gold nanoparticles (Au NPs) in one nanostructure is a promising technique for various applications. Fe_3O_4 NPs have special supermagnetic attributes that allow them to be applied in different areas, and Au NPs stand out in biomaterials due to their oxidation resistance, chemical stability, and unique optical properties. Recent studies have generally defined the physicochemical properties of nanostructures without concentrating on a particular formation strategy. This detailed review provides a summary of the latest research on the formation strategy and applications of Fe_3O_4@Au. The diverse methods of synthesis of Fe_3O_4@Au NPs with different basic organic and inorganic improvements are introduced. The role and applicability of Au coating on the surface of Fe_3O_4 NPs schemes were explored. The 40 most relevant publications were identified and reviewed. The versatility of combining Fe_3O_4@Au NPs as an option for medical application is proven in catalysis, hyperthermia, biomedical imaging, drug delivery and protein separation.

Keywords: inorganic nanoparticles; chemical method; formation strategy; medical applications

Citation: Ali Dheyab, M.; Abdul Aziz, A.; Jameel, M.S.; Moradi Khaniabadi, P. Recent Advances in Synthesis, Medical Applications and Challenges for Gold-Coated Iron Oxide: Comprehensive Study. *Nanomaterials* **2021**, *11*, 2147. https://doi.org/10.3390/nano11082147

Academic Editors: Jihoon Lee and Ming-Yu Li

Received: 26 July 2021
Accepted: 13 August 2021
Published: 23 August 2021

1. Introduction

Coated nanoparticles, or core@shell nanoparticles, consist of two or more nanoparticles that contain a wide variety of organic as well as inorganic nanoparticles, where one serves as a core while the other is centered on the core and named the shell [1]. Knowledge of core@shell synthesis is a pioneering step of nanoscience, as the way to manipulate the nanoparticles' structure has enabled us to generate a variety of hybrid NPs [2,3]. Core@shell NPs, with the potential to be used as core or shell in a wide variety of materials, will reflect their satisfying distinctive properties and custom functions. Core or shell products can be chosen, depending on the intent of the study [4]. The core@shell property can be modified by causing changes to the components that make up the shell layer or core [5]. Characteristics and distinctive attributes such as optical, magnetic, biological, compatibility, chemical stability and physicochemical properties can be realized when different nanoparticles are incorporated, such as gold nanoparticles (Au NPs) on iron oxide nanoparticles (Fe_3O_4 NPs). In recent years, substantial attempts have probably been introduced to evaluate the biomedical applications of Fe_3O_4 NPs, including protein purification, immunoassays, hyperthermia, drug delivery, magnetic resonance imaging (MRI), and computed tomography (CT) [6]. Fe_3O_4 NPs are the most favored nanomaterials in medical applications because of their minimal toxicity features and excellent physicochemical characteristics such as stability, biocompatibility and supermagnetism [7]. The magnetic response stability of Fe_3O_4 is due to its low oxidation sensitivity [8]. In addition, size control, preventing aggregation via coating, precise dispersion and interaction, as well as the penetration of tissue and

cell barriers all give Fe_3O_4 NPs an advantage over other metal nanoparticles. Fe_3O_4 NPs provide a forum for therapeutic uses where they can be utilized for their contrast agent characteristics in MRI diagnostics, as well as for therapeutics in the form of bio-catalysis, drug delivery and protein purification [9].

Various kinds of functional materials, including silica, polymers and Au have been formed on the Fe_3O_4 NPs surface to improve biocompatibility, chemical stability as well as processability for broader applications [10,11]. Au is considered to be the most desired coating material for the production of Fe_3O_4@Au NPs due to its surface functionality, catalytic activity and superior optical properties [12–15]. Because of the variety of physicochemical features and the ability to change the magnetic and optical property by modifying the charge, size, shape, surface modification and thickness of the Au shell, Fe_3O_4@Au NPs have been widely considered the most effective candidature for medical applications [16]. Several studies have been reported for the synthesis of Fe_3O_4@Au NPs. These studies generally described nanoparticles' physicochemical properties without focusing on a specific formation strategy [17–19].

For this reason, the current review will: (1) summarize the latest progress (2018–2020) in the design and synthesis of the Fe_3O_4@Au and elaborate upon the strategies involved in the formation Fe_3O_4@Au NPs core@shell, Fe_3O_4@Au HNPs, Fe_3O_4@Au core@satellite NPs as and as nanodumbbells, Fe_3O_4@Au DNPs; (2) explore the schemes of each manufacturing strategy for Au-coated Fe_3O_4; and (3) present the potency of Fe_3O_4@Au as a promising candidature for medical applications in areas of catalysis, hyperthermia, biomedical imaging, drug delivery and protein separation (2018–2020).

2. Synthesis of Fe_3O_4@Au

Fe_3O_4@Au NPs can be classified as Fe_3O_4@Au NPs core@shell, Fe_3O_4@Au HNPs, Fe_3O_4@Au core@satellite NPs as and as nanodumbbells, Fe_3O_4@Au DNPs structures. In this section, the synthesis of all structures will be introduced.

2.1. Core@Shell Structure of Fe_3O_4@Au

Core@shell nanoparticles have various properties, such as magnetism, metallicity and semiconductivity. These attributes come either through the core or shell materials, or both (Figure 1). In this review, we will discuss Fe_3O_4 NPs as a core and Au NP as a shell.

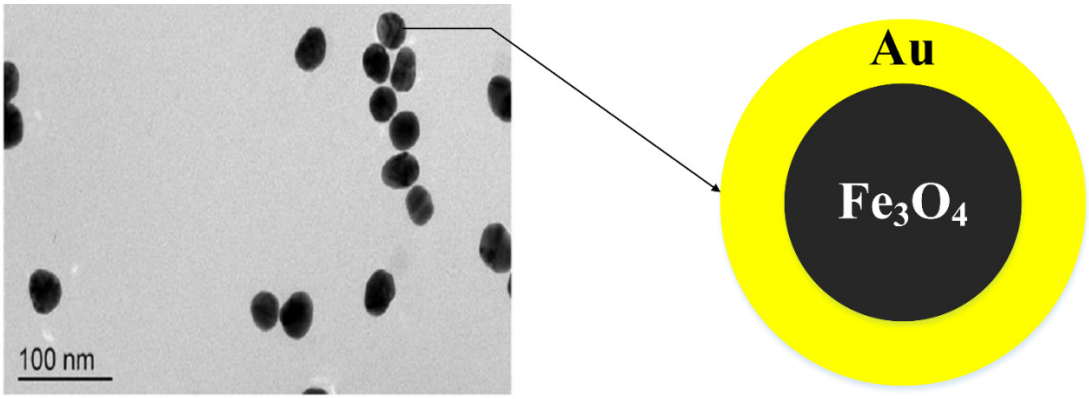

Figure 1. TEM image [20] and schematic diagram of Fe_3O_4@Au NPs core@shell construction.

Recently, Xie et al. [21] have synthesized novel core@shell NPs for use in fast, sensitive, convenient and good surface-enhanced Raman scattering. This method involved two steps for the formation of core@shell NPs: (i) the preparation of Fe_3O_4@silica NPs, using an ultrasound technique to deposit silica oxide on the surface of Fe_3O_4 for 5 min; and (ii) the preparation of the Fe_3O_4@SiO_2@Au seed, using a seed growth method. A similar study was submitted by He et al. [20]. Fe_3O_4@Au NPs were coated with glutathione to reduce the dose dependence of the anticancer medication, doxorubicin (DOX), by covering the glutathione

shell on Fe_3O_4@Au NPs [22]. The former Fe_3O_4@Au NPs produce involved this process. Twenty milliliters (20 mL) of $HAuCl_4$ solution (0.1%) was added to 40 mL of distilled water in a 250 mL flask. The solution was refluxed and Fe_3O_4 was applied to the mixture, then the mixture was boiled for 45 min. A reduction (sodium citrate) was quickly applied under vigorous stirring to the boiling mixture. Citrate addition contributes to the color shift from a grey to a red solution. The solution was boiled for 15 min and then stirred until the solution reached room temperature. The use of glutathione conjugations thus acts as an effective vehicle of drug delivery. In addition to causing drug release with redox-activated glutathione, it requires significantly low levels of glutathione @Au@ Fe_3O_4 NPs for DOX releases. The sonochemical approach effectively synthesizes monodispersive and highly stable Fe_3O_4@Au NPs, with a size distribution of approximately 20 nm during 8 min [23]. Utilizing surface response (RSM) methodology, test runs of 14 dissimilar variations of gold ions, sonication frequency and sodium citrate (independent variables) have been conducted at two-center points to optimize testing procedures. Variance analysis (ANOVA) has been used to achieve optimal conditions for experimental results. The optimal zeta potential value of about –46.125 mV was reached under the ideal conditions of independent variables, which is compatible (at approximately 99.2%) with the real zeta potential value (–45.8 mV). The monodispersity and stability of the Fe_3O_4 NPs effectively coordinated a transition to the core@shell, as demonstrated by a rise in zeta potential value from –24 mV to –45 mV. To date, no work has been reported which produced core@shell NPs for large-scale production. The sonochemical method is widely considered to be one of the most promising methods for preparing, encapsulating and modifying nanoparticles due to its safe, rapid, low-cost and environmentally friendly characteristics [24]. Various types and shapes of nanomaterials have been prepared using a sonochemical method [25,26]. In addition, the sonochemical method ensures the uniformity, homogeneity and monodispersity of the nanoparticles produced [27]. From this point of view, all these advantages and properties of this method may have the potential to be more applicable to large-scale production.

Somayeh et al. [28] carried out a simple and eco-friendly green method for the preparation of spherical Fe_3O_4@Au with a size of 31 nm, utilizing the aqueous extract of the Carum carvi seed which plays three functions such as reduction, capping, and stabilizer agents during the Fe_3O_4@Au synthesis process (Table 1). The seeds of Carum carvi were thoroughly washed with distilled water, followed by drying at 25 °C for 2 days. In the end, the resultant was milled to produce a powder. In order to prepare the aqueous extract, the powder was steeped in 100 mL of distilled water for 10 h at a temperature of 25 °C and then purified using filter paper to acquire a clear solution. To synthesize Fe_3O_4@Au, 50 mg of Fe_3O_4 was dissolved in 100 mL of aqueous extract of Carum carvi and the mixture solution was stirred for around 10 min. Twenty milliliters (20 mL) $HAuCl_4$ solution (5 mM) was then applied to the mixture solution. Finally, the mixture solution was kept for 24 h and then dried overnight at 70 °C. The green, rapid and low-cost preparation of core@shell Fe_3O_4@Au NPs using natural honey as a reducing as well as stabilizing agent through hydrothermal method for 20 min was reported by Rasouli et al. [29]. Fe_3O_4 NPs were dissolved in 50 mL ultrapure water and sonicated for 2 min, to which 25 mL of $HAuCl_4$ (0.005 M) was added and stirred for 15 min to achieve the full adsorption of gold ions on the surface of Fe_3O_4. Subsequently, 0.25 g of the natural honey was added to the mixture solution, held under the hydrothermal method at 120 °C for 20 min. Eventually, Fe_3O_4@Au NPs were separated from the excess result solution using a permeant magnet and washed three times through ultrapure water. TEM images revealed that the synthesis of Fe_3O_4@Au NPs has a diameter ranging between 3.49 and 4.11 nm. Tarhan et al. [30] announced that novel Fe_3O_4@Au NPs, functionalized via maltose, have been prepared as a favorable carrier matrix for easy and efficient L-asparaginase immobilization. The findings show that NPs are monodispersed to 9.0 emu/g magnetization with a size of 10 nm. Tarhan et al. [30] expect that flexible carriers will lead to new possibilities for applications in the fields of biomedicine, biotechnology and biochemistry on the basis of the success of the procedure and the promising findings achieved from their novel process.

Table 1. Summary of the recently published studies on the synthesis methods of Fe_3O_4@Au NPs.

No.	Nanoparticles Structure	Synthesis Method	Size/Shape	Applications	Ref
1	Core@shell	Growth method	5 nm/spherical	Food application	[21]
2	Core@shell	Sonochemical	~40 nm/flower	Food application	[20]
3	Core@shell	Green method	31/spherical	Antimicrobial activity	[28]
4	Core@shell	Green method	3.49–4.11 nm/semispherical	Drug delivery	[29]
5	Core@shell	Reduction	10 nm/amorphous	Enzyme immobilization	[30]
6	Core@shell	Sonochemical	20–50 nm/spherical	Cancer biomarkers	[31]
7	Core@shell	Seeds growth	9.49, 10.04 and 8.95 nm/flower	Catalytic reduction of RhB	[32]
8	Core@shell	Seeding technique	15–57 nm/		[33]
9	Core@shell	Nano-emulsion technique	11 nm/semispherical		[34]
10	Core@shell	Laser ablation	20 nm/spherical		[35]
11	Core@shell	Reduction	20–50 nm/semispherical	Cytotoxicity assay in MDCK cell line	[36]
12	Core@shell	Reduction	~100 nm/flower		[37]
13	HNPs	Reduction	10 nm/spherical	Hyperthermia	[38]
14	Au/PDA hybrid	In situ redox-oxidize polymerization	25 nm/spherical	Catalysis and adsorption	[39]
15	Fe_3O_4@Au@CeO_2 hybrid	Redox reaction	17 nm/nanofibers	Catalysis	[40]
16	HNPs	Thermal decomposition	25 nm/octahedral	Theranostics	[41]
17	HNPs	Seeds growth	90 nm/spiky	Multimodal in vivo imaging	[42]
18	HNPs	Chemical reduction	31 nm/spherical		[43]
19	Core@satellite	Seed-mediated growth	65 nm/cubic	Catalysis	[44]
20	Core@satellite	Hydrothermal treatment, and freeze-drying technologies	300–400 nm/spherical	Microbial fuel cells	[45]
21	Dumbbell NPs	Reduction	22 nm/spherical	Radiation therapy	[46]
22	Dumbbell NPs	Thermal decomposition	7 nm/spherical		[47]

Fe_3O_4@Au NPs have been produced as novel electrochemical immunosensors for the use of cancer biomarkers [31]. The morphology of Fe_3O_4@Au NPs was that of a spherical shape with an average size of approximately 20–50 nm. This novel strategy has shown simpler construction, easier operation and a wider linear range. The proposed approach and the use of a screen-printed carbon electrode provided for the development of a simple electrochemical immunosensor that could be disposable, portable and cheap without using additional labeling. For 15 min under sonication, the suspension of $HAuCl_4$ has been stirred with Fe_3O_4 solution. Subsequently, the reduction agent solution ($NaBH_4$) was quickly added to the cooled suspension, which was then sonicated for another 10 min. Kou et al. [32] reported the custom design of extremely effective catalysts for Fe_3O_4@Au NPs. Fe_3O_4 was formed with three different morphologies using engineered quantities of urea, and the probable mechanism was proposed. Therefore, by measuring the amount of Au

seeds, they achieved Fe_3O_4@Au with different morphologies and tunable Au deposition. The catalytical ability of Fe_3O_4@Au with several structures was compared through the application to degrade 4-nitrophenol and catalytic rhodamine while systematically investigating the correlation of the Au seed amount to the turnover frequency and the catalytic capability of Fe_3O_4@Au. They observed that the flower-like Fe_3O_4@Au NPs with 20 mL of Au seeds applied had the highest degradation rate of 96.7%, and after recycling, their catalytic ability was almost unchanged. The formation of Fe_3O_4@Au NPs was accomplished by reducing the Au ions on the Fe_3O_4 surface using the seeding technique [33]. In a definite volume of glycerin, different concentrations of oxidized Fe_3O_4 or the Au-shell reaction were used. The reaction solution, including the reduction agent and Fe_3O_4 cores, was first sonicated for 15 min, then heated with vigorous stirring to approximately 150 °C. Once the reaction solution reached 150 °C, a drop-specific solution was added for $HAuCl_4$. Fifteen minutes after the addition of Au salts, the heating system was stopped but the stirrer proceeded while the mixture was refreshed at room temperature. The component ratio adaptation allowed the Fe_3O_4@Au NPs particle shell thickness to be tuned. The present route produces well-determined structures of the Fe_3O_4@Au NPs of various sizes between 15 and 57 nm, with the Au noble metal varying from Fe_3O_4 NPs. Bi-phase Fe_3O_4@Au NPs were provided using a nano-emulsion technique [34]. Characterization reveals that the Fe_3O_4@Au nanostructure produced a particle size and distribution of approximately 11 nm in size. The NPs are non-toxic, water-soluble and stable due to the capping agent covering the particles. Optical and magnetic data indicate that the NPs have a narrow-band surface absorption of plasmon and an increased susceptibility to the Au shell. As a result, the bi-phase Fe_3O_4@Au NPs are challenging for various applications such as magnetic separation, optical detection and photonic therapy. In a different process, Au and Fe_3O_4 representing magneto-plasmonic NPs were obtained in two successive steps in an aqueous environment by the laser ablation of the Au and Fe_3O_4 targets [35]. Au NPs are trapped in a Fe_3O_4 mucilaginous matrix, which was established by both microscopic and spectroscopic observation as magnetite. The plasmonic property of the colloids obtained was tested with surface-enhanced Raman scattering spectroscopy, as well as their adsorption capability. In addition to those inherent in Au NPs, the presence of Fe_3O_4 offers the bimetallic colloid new avenues of adsorption, particularly with respect to organic contaminants and heavy metals, allowing them to be extracted from the aqueous environment to promote a magnetic field. In addition, these NPs are low in toxicity, making them promising for biomedical applications. Fe_3O_4@Au in a size range of about 20–50 nm and significant magnetization saturation using a solvothermal one-pot process was recorded by Ángeles-Pascual et al. [36]. $NaBH_4$ gradually reduced the $HAuCl_4$ solution into 9 mL of the black NP solution to create a thin gold shell on the Fe_3O_4 NPs surface. The solution, under intense stirring, was heated up to 70 °C and allowed to naturally cool down to room temperature. Afterwards, Fe_3O_4@Au was separated using the neodymium magnet and rinsed to remove the excess of chemicals from the reagents. To examine the biocompatibility of NPs, a cytotoxicity assay was performed in the MDCK cell line. The tests for the Fe_3O_4@Au NPs exhibited higher cell viability, indicating their excellent biocompatibility and their potential for medical application. A novel and direct method for preparing Fe_3O_4@Au NPs comprising a Fe_3O_4 core coated with an Au shell was identified [37]. The synthesis incorporates ease of operation, minimal control and high reproducibility while at the same time being environmentally friendly. The shell of Au NPs with a controllable thickness of 30 nm was developed on the Fe_3O_4 core of 20 nm in size by reducing Au salt in the ultrasonic bath. Au shell thickness might be adjusted by means of varying the quantity of Au salt applied. Fe_3O_4@Au NPs of sizes ranging between 80 and 160 nm were prepared. The Fe_3O_4@Au NPs were studied for their magnetic and plasmonic behavior. Functionalization with polyethene glycol was conducted to explore its possible use in biomedical applications. Unlike Fe_3O_4@Au DNPs, core@shell was commonly utilized as a contrast agent in dual MR and CT imaging techniques.

2.2. The Hybrid Structure of Fe_3O_4@Au (HNPs)

The synthesis of hybrid Fe_3O_4@Au NPs (HNPs) with appropriate size, design and properties is difficult, and has gained considerable attention among researchers in material sciences. It is possible to tune the design of Fe_3O_4@Au HNPs by selecting the proper technique and controlling the processing parameters during the synthesis.

Fe_3O_4@Au HNPs have single-hybrid nanoparticles consisting of an entire-layer Au ion-reducing coating on the Fe_3O_4 surface. In addition to biocompatibility, the structure of Fe_3O_4@Au HNPs can also impart the NPs surface with appropriate biological and chemical interface activity [48]. A well-defined novel structure can easily be formed by the Au shell uniformly coated on the surface of Fe_3O_4 NPs with sulfur-based ligands. A considerable amount of work has been performed during the last two decades to develop Fe_3O_4@Au HNPs using various techniques, including co-precipitation, seed-mediated growth, direct coating and thermal decomposition methods. The most popular method for preparing Fe_3O_4@Au HNPs is the Au shell's direct coating on the Fe_3O_4 surface. In this approach, two strategies for forming the shell of Au on the Fe_3O_4 surface were observed. The first method is a one-pot process in which the Au ions extend to form the shell on the Fe_3O_4 NPs surface. For the second process, Au NPs are internally produced, then seeded into a suspension of Fe_3O_4 NPs to create Fe_3O_4@Au HNPs [18]. Sood et al. [49] observed that the Au shell's direct coating on the Fe_3O_4 NPs surface loaded with small ligands, including ascorbic acid and citric acid, may be more successful.

Park et al. [38] described the hyperthermic features of Fe_3O_4@Au HNPs within a 200 kHz and 1.5 kA m^{-1} biocompatible alternating magnetic field (AMF). In the air atmosphere, a 0.4 mL precursor of iron was added to a mixture of both oleic acid with octyl ether at 100 °C. The solution was stirred during 1.5 h before being cooled at room temperature. A mixture of oleylamine (0.5 mmol) and $HAuCl_4$ (1.3 mmol) in the 5 mL of chloroform was added two times at intervals of approximately 5 minutes with vigorous stirring with a solvent of oleylamine (2 mmol) and Fe_3O_4 NPs (0.1 mg) in chloroform (10 mL). HNPs were produced by growing Au NPs on the Fe_3O_4 NPs surface with an average size of 10 nm. Due to the decrease in the saturation value of the HNP solution relative to the Fe_3O_4 NPs, the initial heating rate was set to lower than the Fe_3O_4 NPs solution. The continued application of the AMF gradually increased the HNP solution temperature, while the solution of the Fe_3O_4 NPs achieved thermal equilibrium. A similar AMF condition was demonstrated with the heating efficiency of Au NPs combined with non-conductive and diamagnetic SiO_2 NPs, which demonstrates that sustained heat for HNPs may be due to the supplementary heating of the Au NPs in a radiation frequency solenoid belt (RF). A novel hollow nanosphere Fe_3O_4@Au/polydopamine (Au/PDA) capable of absorbing potentially toxic ions plus catalyzing the decrease in 4-nitrophenol has been published [39]. The hybrid shell has well encapsulated the hollow nanosphere Fe_3O_4(Au/PDA) to create the dual-functioning magnetics hollow nanocomposites utilizing an easy redox-oxidizing polymerization technique (Figure 2). Due to its uniform, hollow interior and usable PDA coating with a strong activity of the Au nanoshell, the eventual hollow nanosphere Fe_3O_4@Au/PDA has great potential for drug delivery and nanocatalysis. In brief, the multifunctional Fe_3O_4@Au/PDA nanosphere has wide application potential for coexisting toxic water contamination, green and simple synthesis and ease of manipulation, effective adsorption efficiency and strong catalytic activity. Au NPs play a crucial part in heterogeneous catalytic reactions. Nevertheless, Au NPs typically have low selectivity and complex recyclability. Fe_3O_4@Au@CeO_2 hybrid nanofibers were prepared in the presence of Fe_3O_4 nanofibers, through a simple one-pot redox reaction between $HAuCl_4$ and Ce $(NO_3)_3$ [40]. On the Fe_3O_4 nanofibers' surface, the CeO_2 shell was uniformly coated to form a unique hybrid structure, while the Au NPs were encapsulated within the CeO_2 shell. As a result of the CeO_2 shell formation, Fe_3O_4@Au@CeO_2 hybrid nanofibers are positively charged surfaces, allowing them to be excellent choices for the predominantly sensitive catalytic action against the degradation of negatively charged organic colors. The Fe_3O_4@Au@CeO_2 hybrid nanofibers have demonstrated magnetic properties, giving them good recyclable

usability. This research provides a simple and efficient solution for preparing the hybrid nanomaterials of magnetic noble metal/metal oxide with a distinctive surface characteristic and chemical structure for offering applications in heterogeneous catalysis. A high temperature wet chemical method was used for the synthesis of Fe_3O_4@Au HNPs with a diameter of 25 nm [41]. Fe_3O_4@Au HNPs with Au seeds produced in situ were derived at high temperatures through the thermal decomposition of $HAuCl_4$ and $Fe(CO)_5$. Fe_3O_4@Au HNPs revealed the best features for application as hyperthermic and contrast agents for MRI. Due to the large saturation magnetization and octahedral shape of the magnetite particles, Fe_3O_4@Au HNPs obtained a particular loss power of approximately 617 $W \cdot gFe^{-1}$ with an exceptionally high r_2-relaxivity of about 495 $mM^{-1}s^{-1}$.

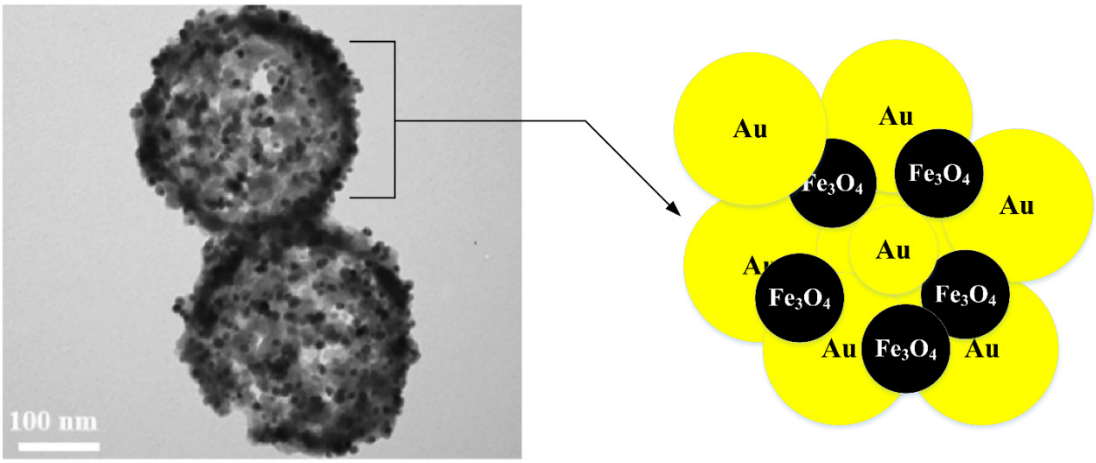

Figure 2. TEM image [39] and schematic illustration for the production of hybrid Fe_3O_4@Au HNP.

Wang et al. [42] stated that the novel structure of spiky Fe_3O_4@Au (SPs) is used for multi-modal imaging and phototherapy agents. The uniformly sized Fe_3O_4@Au SPs were synthesized in two steps. First, citrate-stabilized Fe_3O_4 NPs of the average size of 10 nm was synthesized, then the Au layer was coated on the Fe_3O_4 NPs surface to create Fe_3O_4@Au HNPs, which were used for the production of Fe_3O_4@Au SPs. The SPs exhibit great photodynamic effects and therapeutic photothermal, with a photothermal conversion efficiency of about 31%, and enable tumor-targeted imaging, such as MRI, photoacoustic and computed tomography. The SPs display good biocompatibility, in vivo as well as in vitro. Additionally, the SPs obliterated a tumor below 808 nm of radiation owing to its unique absorption in the near-infrared field. SPs represent a convenient product for application in clinical practice with their potential for deeply integrated multimodal imaging as well as multiple therapeutic functions. Fe_3O_4@Au HNPs have been produced, characterized and presented as a new porous marker to increase micro-/nano-based pores found and quantified by SEM in the shale [43]. With the presynthesized Fe_3O_4 NPs in a solution, the Fe_3O_4@Au HNP shale has been synthesized using the chemical reduction technique. Because of the superparamagnetic properties, the nanomarker is easily operated via the external magnetic field to appoint in pores and provides a sharp contrast picture between the pores and shale matrix, making it much easier and more accurate to recognize micro/nano-sized pores in shales. Moreover, as Au NPs are particularly rare noble metals in the shale, Au's energy-dispersive X-ray mapping was used to accurately calculate area porosity in a shale. A precise and realistic technology is recommended to enable the characterization of micro/nano-pores in the shale in conjunction with the aforementioned merits of the nanomarker. The design and synthesis of hybrid NPs with distinct morphologies can draw the interest of scientists to hybrid biosynthesis NPs.

2.3. Core@Satellite Structures

One of the popular frameworks for Fe_3O_4@Au NPs is core@satellite (Cs). This structure has a single core of Fe_3O_4 with the binding by covalent bonds of numerous Au NPs similar to satellites. The $CsFe_3O_4$@Au NPs comprise a residually exposed core surface of Fe_3O_4 suitable for MR imaging and further functionalization. In addition, the Cs structure consists of many peripheral Au NPs with a large surface area of the satellite nanoparticle that is advantageous for imaging as well as photothermal capabilities [50]. $CsFe_3O_4$@Au NPs are drawn up using different methods. Liu et al. [44] announced that a seed deposition method was used to produce $CsFe_3O_4$@Au nanocubes (Figure 3). Ten milliliters (10 mL) of Au seeds were applied dropwise to obtain Fe_3O_4@PEI nanocubes dispersed in deionized water through ultrasonic treatment. The $CsFe_3O_4$@PEI@Au nanotubes were thoroughly washed with deionized water after 2 h of sonication. Recently, Song et al. [45] succeeded in developing $CsFe_3O_4$@Au NPs that combined three-dimensional microporous graphene foam was formed by an efficient approach which integrated in situ growth, hydrothermal treatment and freeze-drying methods. Ultrasonic treatment was required during the sample preparation to help form a stable mixed colloidal suspension of precursors. Nevertheless, it is notable for Au NPs to be removed from the $CsFe_3O_4$/Au NPs by using ultrasound. The binding force between the products of $CsFe_3O_4$/Au NPs must be powerful enough to solve this problem. As a result, the Cs Fe_3O_4/Au NPs used in this method were provided using an in situ growth technique, where Fe_3O_4 NPs coated with citric acid were utilized as seeds to reduce gold ions ($HAuCl_4$) with the asset of sodium citrate for the nucleation and growth of Au NPs on Fe_3O_4 NPs surfaces.

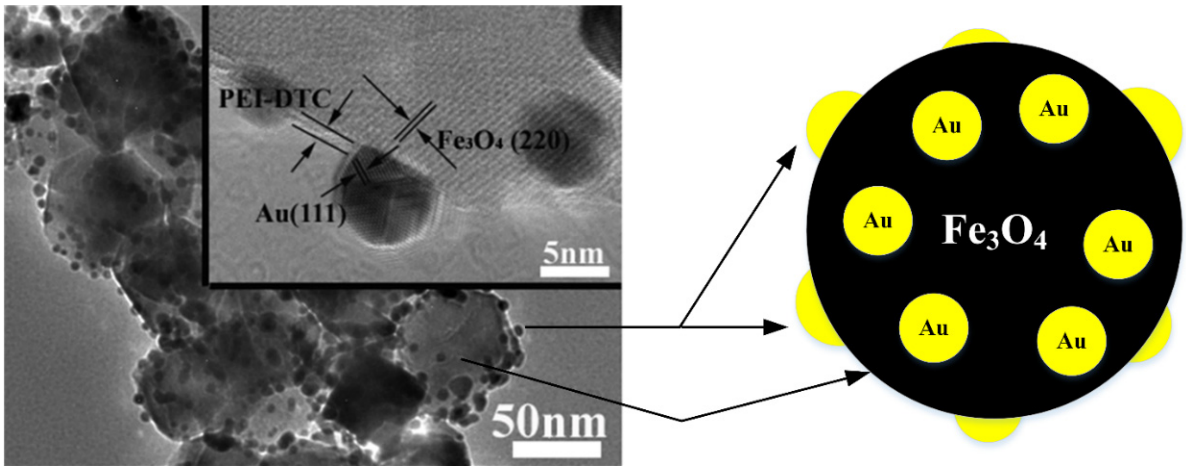

Figure 3. TEM image [44] and schematic diagram for the preparation of core@satellite $CsFe_3O_4$@Au NPs.

2.4. Fe_3O_4@Au Nanodumbbells

Dumbbell NPs (DNPs) consist of a tightly interacting heterostructure together with one NP at the other end (Figure 4). The separate NPs are dumbbell-like or resemble particles in near contact with each other. In contrast to Fe_3O_4@Au HNPs in which Au shields the Fe_3O_4 core, the Fe_3O_4@Au DNP's have a broad-based functional surface and active interface which improves their applications for diagnostics and therapy as theranostics [51]. Fe_3O_4@Au DNPs have unique features, including (1) the ability to allocate various functionalities to delivery applications and particular target imaging; (2) the magnetic detection and simultaneous optical abilities; and (3) the ability to customize optical and magnetic features by adjusting the size of Fe_3O_4@Au HNPs [52]. Fe_3O_4@Au DNPs can be regularly produced through the epitaxial growth of one NP to another form of NPs called NP seed. During the procedure, the nucleation should be properly regulated to generate heterogeneous nucleation on a particular crystalline phase around the seed NPs [53]. Klein et al. [46] developed a simple one-pot synthesis method for the preparation of Fe_3O_4@Au DNPs using a sonication process. In their

analysis, Fe_3O_4@Au DNPs were achieved by the co-precipitation of Fe_3O_4 NPs in an aqueous solution of $HAuCl_4$. Subsequently, 3-mercaptopropionic acid was added to a mixture to stabilize Fe_3O_4@Au DNPs. The resulting DNPs were collected by permanent magnetism and washed three times with 20 mL of ultrapure water. Kostevsek et al. developed Fe_3O_4@Au DNPs coated with chitosan using a two-step process [47]. First, Fe_3O_4@Au DNPs were provided through the reduction of Au ions using the thermal decomposition of the Fe pentacarbonyl ($Fe(CO)_5$) with the existence of oleic acid, oleylamine and 1,2-hexadecanediol at the same time. An Au NP was observed to develop at first in the mixture, during the reaction because of a larger variance in the potential for reduction between Fe and Au. Afterwards, Au NPs were used to break down $Fe(CO)_5$ to produce Fe_3O_4@Au at higher temperatures. Second, the surface of Fe_3O_4@au presynthesized NPs was changed to produce highly biocompatible Fe_3O_4@Au DNPs coated with chitosan, utilizing hydrocaffeic acid and thioglycolic acid-conjugated chitosan. Fe_3O_4@Au DNPs were shown to be biocompatible within a certain range of concentrations that can be employed for optical and magnetic applications in biomedicine [54]. Despite the fact that much work has been expended in the synthesis of Fe_3O_4@Au CNPs for MR@CT imaging applications, the synthesis and development of these nanoparticle systems remain an open area with significant challenges. For example, Fe_3O_4@Au nanodumbbells have not been extensively used for dual-mode MR/CT imaging applications.

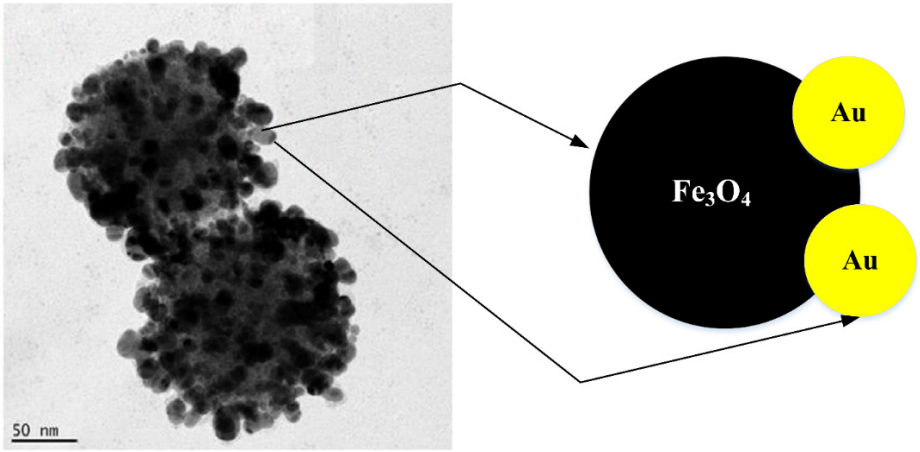

Figure 4. TEM image [55] and schematic drawing of Fe_3O_4@Au DNPs dumbbell preparation.

3. Medical Application of Fe_3O_4@Au NPs

Nanoscience currently ranks among the world's most desirable sciences due to its interdisciplinary research field, which can be used in many applications [55,56]. Fe_3O_4@Au with enhanced properties possesses a specific economic value relative to single NPs due to the current increase in performance, durability and a wide range of industrial, engineering and medical applications. Recently, Fe_3O_4@Au NPs have attracted many researchers due to their wide variety of features, potential, structures, easy control and simple production methods, as discussed above. Fe_3O_4@Au NPs were employed for a wide range of applications, including catalysis [57], hyperthermia [58], biomedical imaging [59], drug delivery [29] and protein separation [60]. Thereby, the most desirable applications will be discussed (Figure 5).

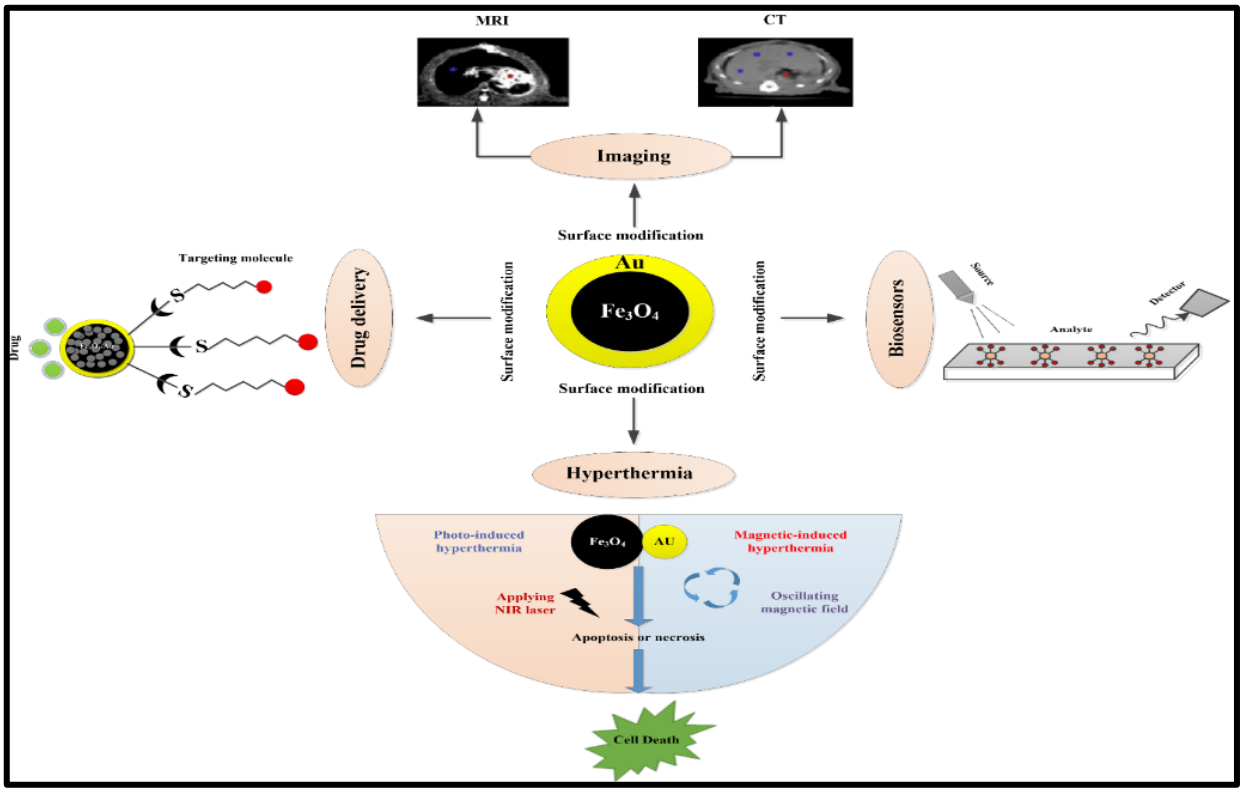

Figure 5. Schematic representation of the medical applications of Fe_3O_4@Au NPs [5].

Izadiyan et al. [61] documented the construction of Fe_3O_4@Au NPs using a modern two-step synthesis technique made of green husk extract from Juglans regia. Their analysis shows that Fe_3O_4/Au NPs' structure, physical and chemical properties exhibit Fe_3O_4 and Au's intrinsic features. The Fe_3O_4@Au NPs display 235 µg/mL of inhibitory concentration $(IC)_{50}$ against colorectal cancer cells (HT-29). Once measured against non-cancer cells, not even up to 500 µg/mL of IC_{50} was obtained. This result exhibited the promising properties of Fe_3O_4@Au NPs for cancer treatment and different biomedical applications. Au shell coating over Fe_3O_4 NPs provides an appropriate platform for adequate modification via therapeutic agents, which is one of the main challenges for the use of Fe_3O_4@Au NPs through cancer therapy. Cancer cells lack the necessary heat-shock reaction and therefore start dying before normal cells when the temperature of the tissue is above 42 °C, and the time necessary to achieve the therapeutic temperature was indeed faster for Fe_3O_4@Au NPs than for naked Fe_3O_4 NPs [36].

Zhao et al. [62] reported the production of Fe_3O_4@Au HNPs at room temperature, which concurrently improved X-ray attenuation as well as showed fluorescence and magnetic properties. Findings from the in vitro fluorescence experiment revealed that the NPs were extremely photostatic and could prevent endosome degradation in cells. Additionally, the in vivo study of normal mice showed 34.61 times more contrast under MR guidance 15 min after the administration of the Fe_3O_4@Au HNPs. The most elevated Hounsfield unit (HU) stood at 174 for 30 min after injections of Fe_3O_4@Au HNPs by CT. In vivo studies of Fe_3O_4@Au HNPs in rat models carrying three different viral infections were further evaluated. For fatty liver models, almost constant contrast improvement was observed without focus dysfunction or nodules under CT and MR (72 HU) and (the highest contrast ratio was 47.33). At the same time, the pronounced enhancement of HCC and cirrhotic liver under CT and MR guidance might be observed in liver parenchyma following Fe_3O_4@Au HNPs injection with highlighted lesions. In addition, the biochemical, hematological and pathological analysis revealed a lack of chronic and acute toxicity and demonstrated the biocompatibility of Fe_3O_4@Au HNPs in vivo applications. These Fe_3O_4@Au HNPs have

shown great potential as a bio-image and multi-modality candidate. Recently, our team recorded Fe_3O_4@Au NPs developed through sonochemical production for MR and CT imaging [63]. The Fe_3O_4 NPs were produced by co-precipitation, followed by the reduction of a gold ion on the Fe_3O_4 surface utilizing a simple and rapid sonochemical process, in just 10 min. Viability testing for a human embryonic kidney cell line (HEK-293) with various doses (100 to 500 Fe µg/mL) for Fe_3O_4 and also Fe_3O_4@Au was performed for various incubation periods (24, 48 and 72 h). Significant reduction in the viability of HEK-293 cells could indeed be identified through an increase in the NPs dose. HEK-293 cells were cultivated with various concentrations of coating NPs (Fe_3O_4@Au), which were higher than that of bare Fe_3O_4 due to the biocompatibility properties of the Au shell. This result means that the Au shells could decrease the toxicity of Fe_3O_4 [64]. Fe_3O_4@Au NPs were first distributed as a control sample in various agar gel concentrations (0.1 to 0.5 mg) using a simple agar gel (Figure 6a). The brightness of the Fe_3O_4@Au NPs MRI images reduces if the dose increases, leading to a decrease in the MRI signal strength via the increasing Fe dose [65]. Transverse relaxivity (r_2) is typically used as a contrast agent to measure the effectiveness of Fe_3O_4. Illustration 6 (b) provides a relaxation rate (T_2) as a variable of the Fe_3O_4@Au NP dose in which T_2 linearly increases during the increase in the Fe dose with an r_2 slope value of about 222.28 mM^{-1} s^{-1} (Table 2). Fe_3O_4@Au NPs' r_2 value is high, probably due to the water protons that can be obtained at the Fe_3O_4 surface of the shell during the interstitial spaces of Au shells. The result of the sensitivity supports the possible use of Fe_3O_4@Au NPs in MRI applications as a T_2-shortening agent. The X-ray attenuation of various concentrations of Fe_3O_4@Au NPs has been studied, employing agar as a sample group to assess the potential of the use of Fe_3O_4@Au NPs as a contrast agent for CT (Figure 6c). The sensitivity of the CT picture improves with the concentration of Au. Illustration 6 (d) exhibits that the Fe_3O_4@Au NPs' CT value (HU) gradually increases with the concentration of Au shell (HU = 418) [66]. This report reveals that the attenuation rate of Fe_3O_4@Au under parallel concentrations of iodine is significantly higher than Omnipaque. This reduction was consistent with an earlier report [66]. Sun et al. stated that because of their higher surface-to-volume ratio, ultrafine Au shells demonstrate higher X-ray attenuation compared to their larger equivalents [67]. This function is imperative since Fe_3O_4@Au NPs' strong X-ray attenuation capability is a prerequisite for their future utilization as a CT contrast agent. In vitro results (r_2 and HU) support the efficacy of Fe_3O_4@Au in MR and CT imaging. In general, Fe_3O_4@Au NPs' MRI contrast influence depends on Fe_3O_4 concentration, whereas the Au shell serves an essential function via the X-ray attenuation of CT imaging.

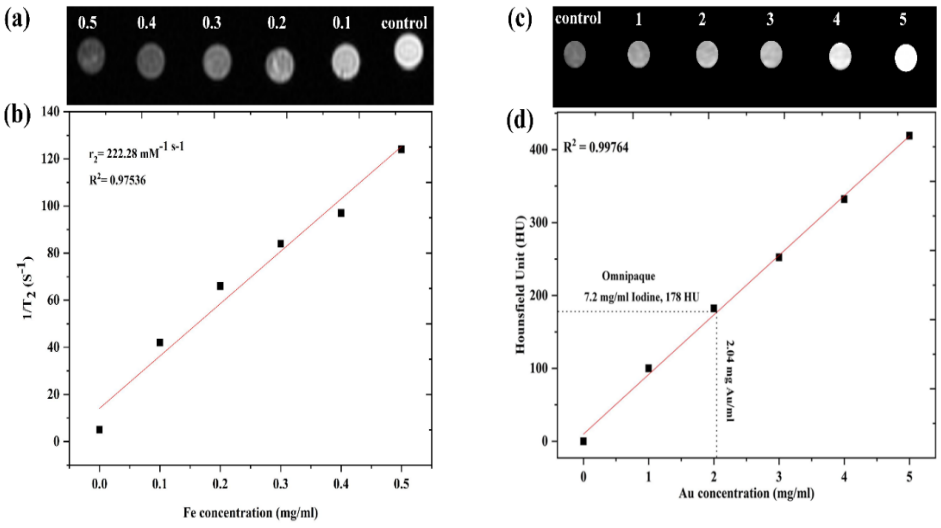

Figure 6. (**a**) MR images with various Fe doses; (**b**) T_2 linear fitting of Fe_3O_4@Au NPs; (**c**) CT images of various Au doses; and (**d**) the intensity of X-ray attenuation [63].

Table 2. Summary of the recently published studies on medical applications of Fe_3O_4@Au NPs.

No.	Nanoparticles Type	Application	Results	Ref
1	Core–shell Fe_3O_4/Au	Anticancer	The Fe_3O_4@Au NPs display 235 μg/mL of inhibitory concentration $(IC)_{50}$ against colorectal cancer cells (HT-29).	[61]
2	Fe_3O_4@Au HNPs	CT-MR dual-modality contrast agents	In vitro phantom studies revealed that these NPs provided superior contrast enhancement for CT and MR imaging.	[62]
3	Fe_3O_4@Au NPs	MRI and CT imaging	The in vitro findings (r_2 = 222.28 mM^{-1} s^{-1}, HU = 418) substantiate the effectiveness of Fe_3O_4@Au NPs in MRI and CT imaging.	[63]
4	Fe_3O_4@Au NPs	Photothermal therapy	The findings demonstrated that Fe_3O_4@Au NPs have the ability to be used as a phototherapeutic agent to enhance the eradication of breast cancer cells.	[68]
5	Fe_3O_4@Au core/shell	Biosensors	Fe_3O_4@Au NPs as new multiplex biosensors of real laboratory testing in complex matrices.	[69]
6	Spiky Fe_3O_4@Au NPs	Theranosticagents	The serum biochemistry results showed that the spiky Fe_3O_4@Au NPs had no discernible toxicity in vivo and could not accurately depict liver and kidney failure.	[70]
7	Fe_3O_4@Au NPs	Dual-modal imaging	The Fe_3O_4@Au NPs proved to be a successful candidate to image tumors for Vivo PA/MR through intravenous injection.	[71]
8	Fe_3O_4@Au NPs	Antibacterial study	Fe_3O_4@Au NPs revealed good antibacterial activity against Gram-positive and Gram-negative pathogens which are found in water.	[72]

Mohammed et al. [68] announced that the sonochemical method successfully synthesized Fe_3O_4@Au with a mean size of 20.8 nm. Fe_3O_4@Au NPs demonstrated slight toxicity to MCF-7 cell lines within 24 h, even with the maximum NPs concentration. The laser irradiation time, power, and wavelength used to treat both cells and NPs were 10 min, 200 mW and 808 nm, respectively. Cell viability decreased dramatically after treatment with 50 μg Fe/mL Fe_3O_4@Au NPs. The findings in this study conclude that Fe_3O_4@Au NPs have the ability to be used as a phototherapeutic agent to improve breast cancer treatment. Fe_3O_4@Au NPs were designed for a plasmon signal enhancement label for nucleotide and serum marker combined detection by Premaratne et al. [69]. The Fe_3O_4@Au NPs' integrated plasmon and magnetic enhancement features proved capable of quickly and magnetically separating the detection-attached sensors and magnifying the SPR signal's performance whilst reducing the non-particular signals of a serum matrix. Such features enhanced the assay's dynamics as well as its selectivity and sensitivity. With the recently developed emphasis on in vitro diagnostic imaging for painless/non-invasive disease and abnormality detection, results showed Fe_3O_4@Au NPs to be new multiplex biosensors of real laboratory testing in complex matrices. Spiky Fe_3O_4@Au NPs were proven to be efficacious theranostic agents in photothermal treatment, a drug-targeted delivery and genetic transmission system [70]. The clearance, biocompatibility and biodistribution of the spiky Fe_3O_4@Au were studied in mice. The organ distributions revealed that the intravenously administered spiky Fe_3O_4@Au NPs were mainly accumulated in the spleen and liver, and the size of the particles significantly affected their actions in vivo. The biochemistry and electron transmission microscopy serum of ultra-histologic structures revealed that spiky Fe_3O_4@Au NPs had no significant in vivo toxicity and did not present a potential risk of kidney and liver dysfunction. Such results lay the groundwork for the development of future theranostic agents. Kang et al. [71] studied the dual-mode imaging of Fe_3O_4@Au NPs as contrast agents for magnetic resonance (MR) and photoacoustic (PA) imaging. MR

imaging offers a time-dependent location for the tumor, while PA imaging demonstrates the presence of high-resolution blood vessels within the tumor. The Fe_3O_4@Au NPs display a greater value of r_2—approximately 329 mM^{-1} s^{-1}. The Fe_3O_4@Au NPs were also added to the tumor-bearing mice of LNCaP as a successful candidate to image tumors for Vivo PA/MR through intravenous injection. MR/PA imagery results in the tumor area show a substantially improved MR/PA image. In multi-modal imaging, the prepared Fe_3O_4/Au NPs will be widely applied. Fe_3O_4@Au NPs were synthesized through the chemical reduction approach [72]. TEM analysis revealed the production of Fe_3O_4@Au with a mean size of approximately 18 nm. The decreased size allows these Fe_3O_4@Au NPs to effectively infiltrate the bacterial crust, resulting in membrane reliability failure. These Fe_3O_4@Au NPs indicate high antibacterial activity in the water against Gram-positive and Gram-negative pathogens. The result achieved showed that the Fe_3O_4@Au NPs were a strong antibacterial agent. Using invented Fe_3O_4@Au NPs in the medical industry is still challenging because the results of clinical trials have yet to be released.

4. Conclusions and Challenges

Fe_3O_4@Au NPs provide numerous possibilities for a powerful platform for medical applications due to their special optical and magnetic properties. Owing to advances in synthesis methods, various forms of Fe_3O_4@Au NPs such as core@shell NPs, core@shell HNPs, core@satellite NPs and dumbbell NPs have recently been explored. The physicochemical characteristics of Fe_3O_4@Au were controlled by manipulating each NP in terms of composition, size, shape and interparticle correlations according to their needs. Fe_3O_4@Au NPs have been commonly regarded as therapeutic agents for various uses due to various functional materials, including catalysis, hyperthermia, biomedical imaging, drug delivery, and protein separation. Nonetheless, the use of Fe_3O_4@Au NPs as a medical agent is still in its infancy and is faced with many doubts and challenges. It is very challenging to develop more effective, smart and secure Fe_3O_4@Au NPs for medical applications. While several Fe_3O_4@Au NPs have been established, translating these components into real clinical applications has not yet been carried out. To address these drawbacks, efforts should be made to produce Fe_3O_4@Au NPs, where each functionality performs in a combined way without affecting other features and functionality. In addition, these components should be precisely applied to long-term toxicity investigations, biodistribution evaluation and several other preclinical tests. Despite these challenges, medical applications based on Fe_3O_4@Au NPs will indeed find real-time applications due to their special features. Collective efforts from researchers from multidisciplinary backgrounds can enhance the success of using Fe_3O_4@Au HNPs as a medical agent.

Author Contributions: Conceptualization, M.A.D. and A.A.A.; methodology, M.A.D., M.S.J. and P.M.K.; software, M.A.D.; validation, M.A.D. and A.A.A.; formal analysis, M.A.D., M.S.J. and P.M.K.; investigation, M.A.D.; resources, M.A.D.; data curation, M.A.D., M.S.J. and P.M.K.; writing—original draft preparation, M.A.D.; writing—review and editing, M.A.D. and A.A.A.; visualization, M.A.D.; supervision, A.A.A.; project administration, A.A.A.; funding acquisition, A.A.A. All authors have read and agreed to the published version of the manuscript.

Funding: This work was funded by the Malaysian Ministry of Higher Education FRGS grant and the APC was funded by (203/PFIZIK/6711678).

Acknowledgments: We would like to thank the academics, authors and researchers at Universiti Sains Malaysia for their efforts which contributed to making this research work readable and the authors would also like to thank the School of Physics of Universiti Sains Malaysia for supporting this research work.

Conflicts of Interest: The authors declare no conflict of interest.

References

1. Dheyab, M.A.; Aziz, A.A.; Jameel, M.S.; Khaniabadi, P.M.; Mehrdel, B. Mechanisms of effective gold shell on Fe_3O_4 core nanoparticles formation using sonochemistry method. *Ultrason. Sonochem.* **2020**, *64*, 104865. [CrossRef]
2. Nasrabadi, H.T.; Abbasi, E.; Davaran, S.; Kouhi, M.; Akbarzadeh, A. Bimetallic nanoparticles: Preparation, properties, and biomedical applications. *Artif. Cell Nanomed. B.* **2016**, *44*, 376–380. [CrossRef]
3. Gawande, M.B.; Goswami, A.; Asefa, T.; Guo, H.; Biradar, A.V.; Peng, D.-L.; Zboril, R.; Varma, R.S. Core–shell nanoparticles: Synthesis and applications in catalysis and electrocatalysis. *Chem. Soc. Rev.* **2015**, *44*, 7540–7590. [CrossRef] [PubMed]
4. Khatami, M.; Alijani, H.Q.; Nejad, M.S.; Varma, R.S. Core@shell Nanoparticles: Greener Synthesis Using Natural Plant Products. *Appl. Sci.* **2018**, *8*, 411. [CrossRef]
5. Dheyab, M.A.; Aziz, A.A.; Jameel, M.S.; Abu Noqta, O.; Mehrdel, B. Synthesis and coating methods of biocompatible iron oxide/gold nanoparticle and nanocomposite for biomedical applications. *Chin. J. Phys.* **2020**, *64*, 305–325. [CrossRef]
6. Jiang, H.; Zeng, X.; He, N.; Deng, Y.; Lu, G.; Li, K. Preparation and biomedical applications of gold-coated magnetic nanocomposites. *J. Nanosci. Nanotechnol.* **2013**, *13*, 1617–1625. [CrossRef]
7. Coricovac, D.-E.; Moacă, E.-A.; Pinzaru, I.; Cîtu, C.; Soica, C.; Mihali, C.-V.; Păcurariu, C.; Tutelyan, V.A.; Tsatsakis, A.; Dehelean, C.-A. Biocompatible Colloidal Suspensions Based on Magnetic Iron Oxide Nanoparticles: Synthesis, Characterization and Toxicological Profile. *Front. Pharmacol.* **2017**, *8*, 154. [CrossRef] [PubMed]
8. Tran, N.; Webster, T.J. Magnetic nanoparticles: Biomedical applications and challenges. *J. Mater. Chem.* **2010**, *20*, 8760–8767. [CrossRef]
9. Shete, P.; Patil, R.; Tiwale, B.; Pawar, S. Water dispersible oleic acid-coated Fe_3O_4 nanoparticles for biomedical applications. *J. Magn. Magn. Mater.* **2015**, *377*, 406–410. [CrossRef]
10. Sousa, J.B.; Ramos-Jesus, J.; Silva, L.; Pereira, C.; De-Los-Santos-Álvarez, N.; Fonseca, R.A.; Miranda-Castro, R.; Delerue-Matos, C.; Júnior, J.R.S.; Barroso, M.F. Fe_3O_4@Au nanoparticles-based magnetoplatform for the HMGA maize endogenous gene electrochemical genosensing. *Talanta* **2020**, *206*, 120220. [CrossRef]
11. Smith, M.; McKeague, M.; DeRosa, M.C. Synthesis, transfer, and characterization of core-shell gold-coated magnetic nanoparticles. *MethodsX* **2019**, *6*, 333–354. [CrossRef]
12. Shiji, R.; Joseph, M.M.; Unnikrishnan, B.; Preethi, G.; Sreelekha, T. Fluorescent gold nanoclusters as a powerful tool for sensing applications in cancer management. In *Advances in Biomaterials for Biomedical Applications*; Springer: Singapore, 2017; pp. 385–428.
13. Rabeea, M.A.; Owaid, M.N.; Aziz, A.A.; Jameel, M.S.; Dheyab, M.A. Mycosynthesis of gold nanoparticles using the extract of Flammulina velutipes, Physalacriaceae, and their efficacy for decolorization of methylene blue. *J. Environ. Chem. Eng.* **2020**, *8*, 103841. [CrossRef]
14. Dheyab, M.A.; Owaid, M.N.; Rabeea, M.A.; Aziz, A.A.; Jameel, M.S. Mycosynthesis of gold nanoparticles by the Portabello mushroom extract, Agaricaceae, and their efficacy for decolorization of Azo dye. *Environ. Nanotechnol. Monit. Manag.* **2020**, *14*, 100312. [CrossRef]
15. Owaid, M.N.; Rabeea, M.A.; Aziz, A.A.; Jameel, M.S.; Dheyab, M.A. Mushroom-assisted synthesis of triangle gold nanoparticles using the aqueous extract of fresh Lentinula edodes (shiitake), Omphalotaceae. *Environ. Nanotechnol. Monit. Manag.* **2019**, *12*, 100270. [CrossRef]
16. Rajkumar, S.; Prabaharan, M. Theranostics Based on Iron Oxide and Gold Nanoparticles for Imaging-Guided Photothermal and Photodynamic Therapy of Cancer. *Curr. Top. Med. Chem.* **2017**, *17*, 1858–1871. [CrossRef]
17. Salihov, S.V.; Ivanenkov, Y.A.; Krechetov, S.P.; Veselov, M.; Sviridenkova, N.V.; Savchenko, A.G.; Klyachko, N.L.; Golovin, Y.I.; Chufarova, N.V.; Beloglazkina, E.K.; et al. Recent advances in the synthesis of Fe_3O_4@Au core/shell nanoparticles. *J. Magn. Magn. Mater.* **2015**, *394*, 173–178. [CrossRef]
18. Sabale, S.; Kandesar, P.; Jadhav, V.; Komorek, R.; Motkuri, R.K.; Yu, X.-Y. Recent developments in the synthesis, properties, and biomedical applications of core/shell superparamagnetic iron oxide nanoparticles with gold. *Biomater. Sci.* **2017**, *5*, 2212–2225. [CrossRef]
19. Sun, S.-N.; Wei, C.; Zhu, Z.-Z.; Hou, Y.-L.; Venkatraman, S.S.; Xu, Z.-C. Magnetic iron oxide nanoparticles: Synthesis and surface coating techniques for biomedical applications. *Chin. Phys. B* **2014**, *23*, 037503. [CrossRef]
20. He, H.; Sun, D.-W.; Pu, H.; Huang, L. Bridging Fe_3O_4@Au nanoflowers and Au@Ag nanospheres with aptamer for ultrasensitive SERS detection of aflatoxin B. *Food Chem.* **2020**, *324*, 126832. [CrossRef]
21. Xie, Y.; Chen, T.; Guo, Y.; Cheng, Y.; Qian, H.; Yao, W. Rapid SERS detection of acid orange II and brilliant blue in food by using Fe_3O_4@Au core–shell substrate. *Food Chem.* **2019**, *270*, 173–180. [CrossRef]
22. Singh, N.; Nayak, J.; Sahoo, S.K.; Kumar, R. Glutathione conjugated superparamagnetic Fe_3O_4-Au core shell nanoparticles for pH controlled release of DOX. *Mater. Sci. Eng. C* **2019**, *100*, 453–465. [CrossRef]
23. Dheyab, M.A.; Aziz, A.A.; Jameel, M.S. Synthesis and optimization of the sonochemical method for functionalizing gold shell on Fe_3O_4 core nanoparticles using response surface methodology. *Surf. Interfaces* **2020**, *21*, 100647. [CrossRef]
24. Dheyab, M.A.; Aziz, A.A.; Khaniabadi, P.M.; Jameel, M.S. Potential of a sonochemical approach to generate MRI-PPT theranostic agents for breast cancer. *Photodiagn. Photodyn. Ther.* **2021**, *33*, 102177. [CrossRef] [PubMed]
25. Xu, H.; Zeiger, B.; Suslick, K. Sonochemical synthesis of nanomaterials. *Chem. Soc. Rev.* **2013**, *42*, 2555–2567. [CrossRef] [PubMed]
26. Pokhrel, N.; Vabbina, P.K.; Pala, N. Sonochemistry: Science and Engineering. *Ultrason. Sonochem.* **2016**, *29*, 104–128. [CrossRef] [PubMed]

27. Dheyab, M.A.; Aziz, A.A.; Khaniabadi, P.M.; Jameel, M.S.; Ahmed, N.M.; Ali, A.T. Distinct advantages of using sonochemical over laser ablation methods for a rapid-high quality gold nanoparticles production. *Mater. Res. Express* **2021**, *8*, 015009. [CrossRef]
28. Mirsadeghi, S.; Zandavar, H.; Yousefi, M.; Rajabi, H.R.; Pourmortazavi, S.M. Green-photodegradation of model pharmaceutical contaminations over biogenic Fe_3O_4/Au nanocomposite and antimicrobial activity. *J. Environ. Manag.* **2020**, *270*, 110831. [CrossRef] [PubMed]
29. Rasouli, E.; Basirun, W.J.; Johan, M.R.; Rezayi, M.; Darroudi, M.; Shameli, K.; Shanavaz, Z.; Akbarzadeh, O.; Izadiyan, Z. Facile and greener hydrothermal honey-based synthesis of Fe_3O_4/Au core/shell nanoparticles for drug delivery applications. *J. Cell. Biochem.* **2019**, *120*, 6624–6631. [CrossRef] [PubMed]
30. Tarhan, T.; Ulu, A.; Sariçam, M.; Çulha, M.; Ates, B. Maltose functionalized magnetic core/shell Fe_3O_4@Au nanoparticles for an efficient L-asparaginase immobilization. *Int. J. Biol. Macromol.* **2020**, *142*, 443–451. [CrossRef] [PubMed]
31. Butmee, P.; Tumcharern, G.; Thouand, G.; Kalcher, K.; Samphao, A. An ultrasensitive immunosensor based on manganese dioxide-graphene nanoplatelets and core shell Fe_3O_4@Au nanoparticles for label-free detection of carcinoembryonic antigen. *Bioelectrochemistry* **2020**, *132*, 107452. [CrossRef]
32. Kou, Y.; Wu, T.; Xing, G.; Huang, X.; Han, D.; Yang, S.; Guo, C.; Gao, W.; Yang, J.; Liu, Y.; et al. Highly efficient and recyclable catalyst: Porous Fe_3O_4–Au magnetic nanocomposites with tailored synthesis. *Nanotechnology* **2020**, *31*, 225701. [CrossRef]
33. Al-Sherbini, A.-S.A.; El-Ghannam, G.; Yehya, H.; Nassef, O.A. Optical and Magnetic Studies of Fe_3O_4/Au Core/Shell Nanocomposites. *Int. J. Nanosci.* **2019**, *18*, 1850033. [CrossRef]
34. Ma, C.; Shao, H.; Zhan, S.; Hou, P.; Zhang, X.; Chai, Y.; Liu, H. Bi-phase dispersible Fe_3O_4@Au core–shell multifunctional nanoparticles: Synthesis, characterization and properties. *Compos. Interfaces* **2019**, *26*, 537–549. [CrossRef]
35. Muniz-Miranda, M.; Muniz-Miranda, F.; Giorgetti, E. Spectroscopic and Microscopic Analyses of Fe_3O_4/Au Nanoparticles Obtained by Laser Ablation in Water. *Nanomaterials* **2020**, *10*, 132. [CrossRef]
36. Ángeles-Pascual, A.; Piñón-Hernández, J.; Estevez-González, M.; Pal, U.; Velumani, S.; Pérez, R.; Esparza, R. Structure, magnetic and cytotoxic behaviour of solvothermally grown Fe_3O_4@Au core-shell nanoparticles. *Mater. Charact.* **2018**, *142*, 237–244. [CrossRef]
37. Billen, A.; de Cattelle, A.; Jochum, J.K.; Van Bael, M.J.; Billen, J.; Seo, J.W.; Brullot, W.; Koeckelberghs, G.; Verbiest, T. Novel synthesis of superparamagnetic plasmonic core-shell iron oxide-gold nanoparticles. *Phys. B Condens. Matter* **2019**, *560*, 85–90. [CrossRef]
38. Park, S.-I.; Chung, S.-H.; Kim, H.-C.; Lee, S.G.; Lee, S.J.; Kim, H.; Kim, H.; Jeong, S.W. Prolonged heating of Fe_3O_4–Au hybrid nanoparticles in a radiofrequency solenoid coil. *Colloids Surf. A* **2018**, *538*, 304–309. [CrossRef]
39. Xu, K.; Wu, J.; Fang, Q.; Bai, L.; Duan, J.; Li, J.; Xu, H.; Hui, A.; Hao, L.; Xuan, S. Magnetically separable h-Fe_3O_4@Au/polydopamine nanosphere with a hollow interior: A versatile candidate for nanocatalysis and metal ion adsorption. *Chem. Eng. J.* **2020**, *398*, 125571. [CrossRef]
40. Chen, S.; Qiu, S.; Zhong, M.; Tian, D.; Wang, C.; Lu, X. Constructing magnetic Fe_3O_4-Au@CeO_2 hybrid nanofibers for selective catalytic degradation of organic dyes. *Appl. Organomet. Chem.* **2019**, *33*, e5253. [CrossRef]
41. Efremova, M.V.; Nalench, Y.A.; Myrovali, E.; Garanina, A.; Grebennikov, I.S.; Gifer, P.K.; Abakumov, M.; Spasova, M.; Angelakeris, M.; Savchenko, A.G.; et al. Size-selected Fe_3O_4–Au hybrid nanoparticles for improved magnetism-based theranostics. *Beilstein J. Nanotechnol.* **2018**, *9*, 2684–2699. [CrossRef]
42. Wang, W.; Hao, C.; Sun, M.; Xu, L.; Xu, C.; Kuang, H. Spiky Fe_3O_4@Au Supraparticles for Multimodal In Vivo Imaging. *Adv. Funct. Mater.* **2018**, *28*, 1800310. [CrossRef]
43. Li, N.; Zhong, T.; Liu, J.-L.; Zheng, J.; Deng, H.-C.; Zhou, W.; Li, M.; Feng, M.-S.; Liu, Q.-J.; Li, C.-Y.; et al. Precise Identification and Analysis of Micro/Nano-Sized Pore Structure in Shale with Fe_3O_4/Au Hybrid Nanocomposite. *Anal. Chem.* **2018**, *90*, 12706–12713. [CrossRef]
44. Liu, Y.; Zhang, Y.; Kou, Q.; Wang, D.; Han, D.; Lu, Z.; Chen, Y.; Chen, L.; Wang, Y.; Yang, J.; et al. Fe_3O_4/Au binary nanocrystals: Facile synthesis with diverse structure evolution and highly efficient catalytic reduction with cyclability characteristics in 4-nitrophenol. *Powder Technol.* **2018**, *338*, 26–35. [CrossRef]
45. Song, R.-B.; Zhou, S.; Guo, D.; Li, P.; Jiang, L.-P.; Zhang, J.-R.; Wu, X.; Zhu, J.-J. Core/Satellite Structured Fe_3O_4/Au Nanocomposites Incorporated with Three-Dimensional Macroporous Graphene Foam as a High-Performance Anode for Microbial Fuel Cells. *ACS Sustain. Chem. Eng.* **2019**, *8*, 1311–1318. [CrossRef]
46. Klein, S.; Hübner, J.; Menter, C.; Distel, L.V.R.; Neuhuber, W.; Kryschi, C. A Facile One-Pot Synthesis of Water-Soluble, Patchy Fe_3O_4-Au Nanoparticles for Application in Radiation Therapy. *Appl. Sci.* **2019**, *9*, 15. [CrossRef]
47. Kostevsek, N.; Locatelli, E.; Garrovo, C.; Arena, F.; Monaco, I.; Nikolov, I.P.; Sturm, S.; Rozman, K.Z.; Lorusso, V.; Giustetto, P.; et al. The one-step synthesis and surface functionalization of dumbbell-like gold–iron oxide nanoparticles: A chitosan-based nanotheranostic system. *Chem. Commun.* **2016**, *52*, 378–381. [CrossRef] [PubMed]
48. Silva, S.M.; Tavallaie, R.; Sandiford, L.; Tilley, R.; Gooding, J.J. Gold coated magnetic nanoparticles: From preparation to surface modification for analytical and biomedical applications. *Chem. Commun.* **2016**, *52*, 7528–7540. [CrossRef]
49. Sood, A.; Arora, V.; Shah, J.; Kotnala, R.; Jain, T.K. Multifunctional gold coated iron oxide core-shell nanoparticles stabilized using thiolated sodium alginate for biomedical applications. *Mater. Sci. Eng. C* **2017**, *80*, 274–281. [CrossRef]
50. Leung, K.C.-F.; Xuan, S.; Zhu, X.; Wang, D.; Chak, C.-P.; Lee, S.-F.; Ho, W.K.-W.; Chung, B.C.-T. Gold and iron oxide hybrid nanocomposite materials. *Chem. Soc. Rev.* **2012**, *41*, 1911–1928. [CrossRef]

51. Huang, Q.; Li, W.; Lin, Q.; Pi, D.; Hu, C.; Shao, C.; Zhang, H. A review of significant factors in the synthesis of hetero-structured dumbbell-like nanoparticles. *Chin. J. Catal.* **2016**, *37*, 681–691. [CrossRef]
52. Liu, J.; Zhang, W.; Zhang, H.-L.; Yang, Z.; Li, T.; Wang, B.; Huo, X.; Wang, R.; Chen, H. A multifunctional nanoprobe based on Au–Fe_3O_4 nanoparticles for multimodal and ultrasensitive detection of cancer cells. *Chem. Commun.* **2013**, *49*, 4938. [CrossRef]
53. Wang, C.; Xu, C.; Zeng, H.; Sun, S. Recent Progress in Syntheses and Applications of Dumbbell-like Nanoparticles. *Adv. Mater.* **2009**, *21*, 3045–3052. [CrossRef]
54. Gupta, A.K.; Naregalkar, R.R.; Vaidya, V.D.; Gupta, M. Recent advances on surface engineering of magnetic iron oxide nanoparticles and their biomedical applications. *Nanomedicine* **2007**, *2*, 23–39. [CrossRef]
55. Zhao, X.; Zeng, L.; Hosmane, N.; Gong, Y.; Wu, A. Cancer cell detection and imaging: MRI-SERS bimodal splat-shaped Fe_3O_4/Au nanocomposites. *Chin. Chem. Lett.* **2019**, *30*, 87–89. [CrossRef]
56. Rajkumar, S.; Prabaharan, M. Multi-functional core-shell Fe_3O_4@Au nanoparticles for cancer diagnosis and therapy. *Colloids Surf. B* **2019**, *174*, 252–259.
57. Sarno, M.; Iuliano, M. Highly active and stable Fe_3O_4/Au nanoparticles supporting lipase catalyst for biodiesel production from waste tomato. *Appl. Surf. Sci.* **2019**, *474*, 135–146. [CrossRef]
58. Ge, Y.; Zhong, Y.; Ji, G.; Lu, Q.; Dai, X.; Guo, Z.; Zhang, P.; Peng, G.; Zhang, K.; Li, Y. Preparation and characterization of Fe_3O_4@Au-C225 composite targeted nanoparticles for MRI of human glioma. *PLoS ONE* **2018**, *13*, e0195703. [CrossRef]
59. Ding, L.; Wang, R.; Hu, Y.; Xu, F.; Zhang, N.; Cao, X.; Wang, X.; Shi, X.; Guo, R. Folic acid-modified Laponite®-stabilized Fe_3O_4 nanoparticles for targeted T2-weighted MR imaging of tumor. *Appl. Clay Sci.* **2020**, *186*, 105447. [CrossRef]
60. Karami, C.; Taher, M.A. A catechol biosensor based on immobilizing laccase to Fe_3O_4@Au core-shell nanoparticles. *Int. J. Biol. Macromol.* **2019**, *129*, 84–90. [CrossRef]
61. Izadiyan, Z.; Shameli, K.; Miyake, M.; Teow, S.-Y.; Peh, S.-C.; Mohamad, S.E.; Taib, S.H.M. Green fabrication of biologically active magnetic core-shell Fe_3O_4/Au nanoparticles and their potential anticancer effect. *Mater. Sci. Eng. C* **2019**, *96*, 51–57. [CrossRef]
62. Zhao, H.Y.; Liu, S.; He, J.; Pan, C.C.; Li, H.; Zhou, Z.Y.; Ding, Y.; Huo, D.; Hu, Y. Synthesis and application of strawberry-like Fe_3O_4-Au nanoparticles as CT-MR dual-modality contrast agents in accurate detection of the progressive liver disease. *Biomaterials* **2015**, *51*, 194–207. [CrossRef] [PubMed]
63. Dheyab, M.A.; Aziz, A.A.; Jameel, M.S.; Abu Noqta, O.; Khaniabadi, P.M.; Mehrdel, B. Excellent relaxivity and X-ray attenuation combo properties of Fe_3O_4@Au CSNPs produced via Rapid sonochemical synthesis for MRI and CT imaging. *Mater. Today Commun.* **2020**, *25*, 101368. [CrossRef]
64. Keshtkar, M.; Shahbazi-Gahrouei, D.; Mehrgardi, M.; Aghaei, M.; Khoshfetrat, S. Synthesis and Cytotoxicity Assessment of Gold-coated Magnetic Iron Oxide Nanoparticles. *J. Biomed. Phys. Eng.* **2018**, *8*, 357–364.
65. Nosrati, H.; Salehiabar, M.; Kheiri Manjili, H.; Davaran, S.; Danafar, H. Theranostic nanoparticles based on magnetic nanoparticles: Design, preparation, characterization, and evaluation as novel anticancer drug carrier and MRI contrast agent. *Drug Dev. Ind. Pharm.* **2018**, *44*, 1668–1678. [CrossRef] [PubMed]
66. Li, J.; Zheng, L.; Cai, H.; Sun, W.; Shen, M.; Zhang, G.; Shi, X. Facile One-Pot Synthesis of Fe_3O_4@Au Composite Nanoparticles for Dual-Mode MR/CT Imaging Applications. *ACS Appl. Mater. Interfaces* **2013**, *5*, 10357–10366. [CrossRef] [PubMed]
67. Xu, C.; Tung, G.A.; Sun, S. Size and Concentration Effect of Gold Nanoparticles on X-ray Attenuation As Measured on Computed Tomography. *Chem. Mater.* **2008**, *20*, 4167–4169. [CrossRef]
68. Dheyab, M.; Aziz, A.; Jameel, M.; Khaniabadi, P.; Mehrdel, B.; Khaniabadi, B. Gold-coated iron oxide nanoparticles as a potential photothermal therapy agent to enhance eradication of breast cancer cells. *J. Phys. Conf. Ser.* **2020**, *1497*, 012003. [CrossRef]
69. Premaratne, G.; Dharmaratne, A.C.; Al Mubarak, Z.H.; Mohammadparast, F.; Andiappan, M.; Krishnan, S. Multiplexed surface plasmon imaging of serum biomolecules: Fe_3O_4@Au Core/shell nanoparticles with plasmonic simulation insights. *Sens. Actuators B Chem.* **2019**, *299*, 126956. [CrossRef]
70. Zhou, H.; Oh, S.; Kim, J.E.; Zou, F.; Hwang, D.Y.; Lee, J. In Vivo Study of Spiky Fe_3O_4@Au Nanoparticles with Different Branch Lengths: Biodistribution, Clearance, and Biocompatibility in Mice. *ACS Appl. Bio Mater.* **2019**, *2*, 163–170. [CrossRef]
71. Kang, N.; Xu, D.; Han, Y.; Lv, X.; Chen, Z.; Zhou, T.; Ren, L.; Zhou, X. Magnetic targeting core/shell Fe_3O_4/Au nanoparticles for magnetic resonance/photoacoustic dual-modal imaging. *Mater. Sci. Eng. C* **2019**, *98*, 545–549. [CrossRef]
72. Jency, D.A.; Sathyavathi, K.; Umadevi, M.; Parimaladevi, R. Enhanced bioactivity of Fe_3O_4-Au nanocomposites—A comparative antibacterial study. *Mater. Lett.* **2020**, *258*, 126795. [CrossRef]